nature materials

ARTICLES

PUBLISHED ONLINE: 23 FEBRUARY 2015 | DOI: 10.1038/NMAT4219

A photoreversible protein-patterning approach for guiding stem cell fate in three-dimensional gels

Cole A. DeForest[1,2]* and David A. Tirrell[1]*

Although biochemically patterned hydrogels are capable of recapitulating many critical aspects of the heterogeneous cellular niche, exercising spatial and temporal control of the presentation and removal of biomolecular signalling cues in such systems has proved difficult. Here, we demonstrate a synthetic strategy that exploits two bioorthogonal photochemistries to achieve reversible immobilization of bioactive full-length proteins with good spatial and temporal control within synthetic, cell-laden biomimetic scaffolds. A photodeprotection–oxime-ligation sequence permits user-defined quantities of proteins to be anchored within distinct subvolumes of a three-dimensional matrix, and an ortho-nitrobenzyl ester photoscission reaction facilitates subsequent protein removal. By using this approach to pattern the presentation of the extracellular matrix protein vitronectin, we accomplished reversible differentiation of human mesenchymal stem cells to osteoblasts in a spatially defined manner. Our protein-patterning approach should provide further avenues to probe and direct changes in cell physiology in response to dynamic biochemical signalling.

Synthetic hydrogels have emerged as powerful *in vitro* cell culture platforms, providing simplified, near-physiological, three-dimensional (3D) environments in which biological function can be assayed in response to user-defined physicochemical signals[1–3]. By specifying the bulk properties of these constructs through control of the conditions of gel formation, researchers have examined the effects of cell–microenvironment interactions in materials that present biochemical and biophysical cues analogous to those found *in vivo*. These systems have had significant impact on our understanding of many biological processes, including the effects of material stiffness on lineage-specific differentiation[4–6], of cell geometry on proliferation and apoptosis[7], and of culture dimensionality on therapeutic response[8]. Despite their utility, these static platforms cannot capture the spatial and temporal variation with which physiological cues are presented to cells *in vivo*[9]. Such variable signal presentation is critical to many biological phenomena, including tissue morphogenesis, disease progression, and wound healing[10]. Furthermore, dynamic biochemical signalling has been implicated in the determination of stem cell fate[11]. Well-designed *in vitro* platforms capable of recapitulating the dynamic heterogeneity of natural tissue are needed for fundamental biological studies as well for the further development of effective strategies for tissue engineering.

To emulate physiological changes in extracellular matrix (ECM) composition, investigators have focused on photopatterned introduction of biochemical signalling molecules into hydrogels[12]. Because the extent of network functionalization can be altered in time and space through light exposure, photochemical processes provide powerful tools for controlled presentation of molecular signals. Vinyl chain polymerization[13,14], thiol-ene addition[15–17], photocaged thiols that undergo Michael-type chemistry[18,19], photo-induced copper-catalysed azide–alkyne cycloaddition[20], and most recently a light-activated enzymatic crosslinking reaction[21] have each been exploited to decorate synthetic ECMs with signalling ligands. Photocleavage reactions have also enabled controlled removal of biochemical cues from 3D hydrogels, either by the release of biomolecules linked to the substrate through photoscissile bonds[22–24] or by means of bulk photodegradation[22,25–29]. Although these techniques have been used to direct a variety of cellular functions, better control would be afforded by approaches that permit biological cues to be both introduced and subsequently removed. Recently, the use of wavelength-specific photocoupling and photocleavage chemistries to achieve reversible attachment of short peptides to engineered hydrogels has been reported[30]. These methodologies require patterning agents to contain one and only one thiol moiety (for example, a cysteine residue), thereby limiting reversible gel modification to simple, highly engineered small molecules and peptides. Given the increased specificity of proteins and their ability to modulate complex cellular behaviour including stem cell differentiation, protein secretion and cell–cell interactions[31,32], our interest has focused on the related challenge of controlling the reversible presentation of full-length proteins in three-dimensional hydrogel environments[30,31].

Several design criteria have guided our thinking: the approach must allow attachment and subsequent removal of full-length proteins with good control in space and time; all chemistries must be cytocompatible and bioorthogonal, enabling mild and specific bioconjugation and cleavage to be performed on fragile proteins and in the presence of live cells; and patterning must be executed on timescales that are relevant to the biological functions of interest. An approach that satisfies these requirements would yield a new generation of spatially and temporally programmable biomaterials.

Here we describe a combination of three bioorthogonal chemistries that enables reversible, patterned presentation of full-length proteins within polymeric hydrogels (Fig. 1): a strain-promoted azide–alkyne cycloaddition (SPAAC) reaction for network formation, a photodeprotection–oxime-ligation sequence for protein introduction, and an ortho-nitrobenzyl ester photoscission reaction for subsequent protein removal. Hydrogels were formed through SPAAC (ref. 33) between a four-arm poly(ethylene glycol) tetrabicyclononyne (PEG-tetraBCN,

[1]Division of Chemistry and Chemical Engineering California Institute of Technology, 1200 East California Boulevard, Pasadena, California 91125, USA. [2]Department of Chemical Engineering, University of Washington, 4000 15th Avenue NE, Seattle, Washington 98195, USA. *e-mail: profcole@uw.edu; tirrell@caltech.edu

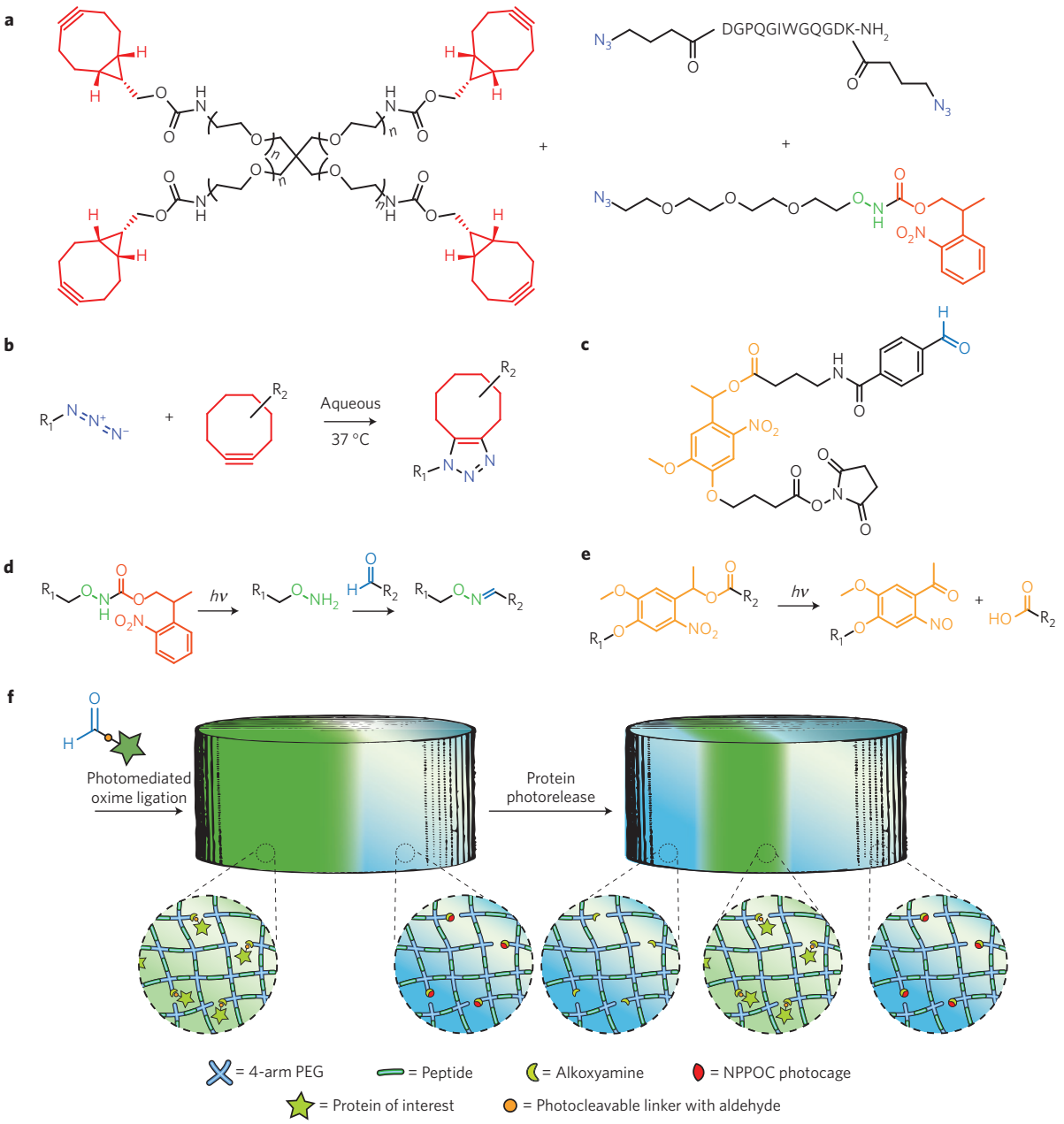

Figure 1 | Hydrogel components and reactions used for photoreversible protein patterning. a, Azide- and alkyne-functionalized precursors react by means of step-growth polymerization to form enzymatically degradable, poly(ethylene glycol)-based 3D hydrogels decorated uniformly with NPPOC-photocaged alkoxyamines. **b**, Gelation occurs through strain-promoted azide–alkyne cycloaddition (SPAAC). **c**, Treatment of proteins with NHS-*o*NB-CHO imparts photopatternability through introduction of reactive aldehydes linked through photoscissile *o*-nitrobenzyl ester (*o*NB) moieties. **d**, NPPOC-caged alkoxyamines distributed uniformly throughout hydrogels (R_1) undergo irreversible β-elimination on exposure to ultraviolet light ($\lambda = 365$ or 740 nm). The liberated alkoxyamines react with aldehyde-functionalized proteins (R_2) to form oxime linkages. **e**, *o*-nitrobenzyl ester (*o*NB) moieties linking the protein of interest (R_1) and the hydrogel (R_2) undergo photocleavage on exposure to ultraviolet light ($\lambda = 365$ nm or 740 nm). **f**, Schematic of the photoreversible patterning strategy, in which NHS-*o*NB-CHO-functionalized proteins are first tethered to the gel through photomediated oxime ligation and subsequently removed on further light exposure.

$M_n \sim 10{,}000$ Da) and an azide-functionalized synthetic peptide (N_3–DGPQGIWGQGDK(N_3)–NH_2) susceptible to cleavage[34,35] by cell-secreted matrix metalloproteinases (Fig. 1a,b and Supplementary Methods 1–3). Although SPAAC has been used in the past to make gels[15], the strategy described here employs a bicyclononyne (BCN) that is synthetically tractable and highly transparent at wavelengths commonly used to initiate photochemical processes. In these respects, the BCN crosslinker offers important advantages over the previously used (di)fluorinated cyclooctynes[36,37] and dibenzocyclooctynes[38,39]. The reaction proceeds quickly; gelation occurs within ~5 min of mixing and yields homogeneous networks with moduli that can be varied from 1 to 10 kPa (Supplementary Fig. 1). The uniformity of the gels facilitates control of protein patterning steps that depend on diffusion, and that can be difficult to control in heterogeneous materials (for example, chain growth systems)[40].

After network formation, photopatterned oxime ligation was used to introduce aldehyde-functionalized proteins at specific locations in the gel (Figs 1d and 2). Despite its status as one of few spatially controllable bioorthogonal chemistries, light-

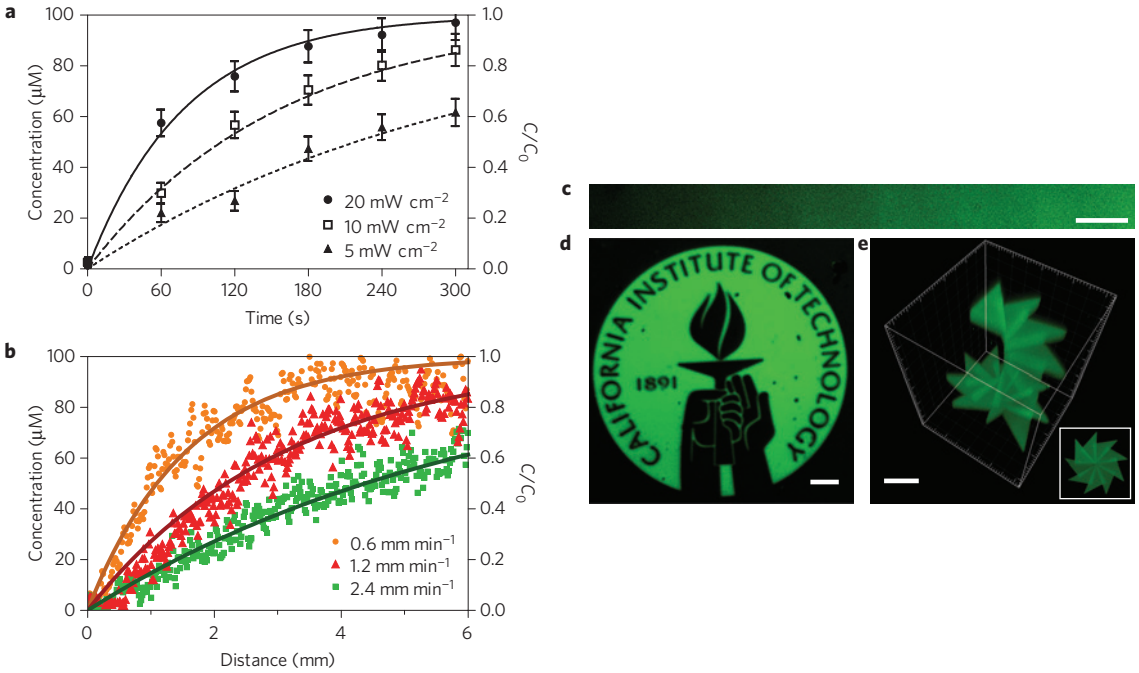

Figure 2 | Patterning of proteins into SPAAC-based gels by means of photomediated oxime ligation. Photoliberated alkoxyamines react with aldehyde-functionalized proteins to form oxime linkages patterned throughout the gel. **a**, By controlling the degree of NPPOC uncaging ($C_0 = 100\,\mu M$) through variation in light intensity (5, 10, 20 mW cm^{-2}, $\lambda = 365$ nm) and exposure time (0–300 s), protein immobilization was varied within wide limits. Data points in **a** correspond to mean values of three independent experimental replicates. Error bars correspond to the standard deviation about the mean. **b**,**c**, Exponential protein gradients were generated predictably by exposing gel surfaces to linear gradients of light exposure, created by covering samples with an opaque photomask moving at different rates (0.6, 1.2, 2.4 mm min^{-1}). **d**, Photolithography ($\lambda = 365$ nm) was used to immobilize proteins in discrete patterns throughout the gel thickness. **e**, Multiphoton laser-scanning lithography ($\lambda = 740$ nm) enabled 3D control over protein immobilization. All studies were performed with BSA_{488}-*o*NB-CHO and all gels were analysed using fluorescence confocal microscopy. In **a**,**b**, lines represent predicted immobilization concentrations based on NPPOC photoscission kinetics. Inset in **e** represents a maximum-intensity *z*-projection. Scale bars, 500 μm (**c**), 100 μm (**d**) and 150 μm (**e**).

assisted conjugation of alkoxyamines and aldehydes has been used previously only to effect the attachment of small molecules to glass surfaces[41,42]. We believe that the experiments described here represent the first use of this chemistry for controlled immobilization of proteins. By including a heterobifunctional 2-(2-nitrophenyl)propyloxycarbonyl (NPPOC)-photocaged alkoxyamine/azide tri(ethylene glycol)-based linker (N_3–TEG–ONH–NPPOC, Fig. 1a and Supplementary Methods 4) in the gel formulation, we introduced caged sites for protein anchoring uniformly throughout the network. On exposure to cytocompatible ultraviolet (UV) light ($\lambda = 365$ nm), the NPPOC-protected linker undergoes an irreversible β-elimination to yield the aldehyde-reactive alkoxyamine[43] (Fig. 1d).

The photokinetics of alkoxyamine uncaging were established through small molecule ^{1}H-NMR studies of N_3–TEG–ONH–NPPOC (Supplementary Fig. 2). The deprotection reaction was found to exhibit first-order photolysis kinetics:

$$C = C_0 e^{-kt}$$

where C is the concentration of intact NPPOC photocage at time t, C_0 is the initial concentration of the NPPOC-protected linker, and k is the rate constant given by:

$$k = \frac{\phi \varepsilon I}{N_A h \nu}$$

where ϕ is the quantum yield (determined to be 0.73 for N_3–TEG–ONH–NPPOC, Supplementary Fig. 2), ε is the molar absorptivity of the sample (measured at 285 M^{-1} cm^{-1} for N_3–TEG–ONH–NPPOC for $\lambda = 365$ nm, Supplementary Fig. 3), I is the intensity of light, N_A is Avogadro's number, h is the Planck constant, and ν is the frequency of the associated electromagnetic wave[44]. The rate expression can be used to predict the amount of alkoxyamine generated under various conditions of light exposure, thereby establishing an upper limit for potential biochemical immobilization by oxime ligation.

Exposure of the gel to patterned UV light causes local uncaging of alkoxyamines and enables subsequent attachment of carbonyl-functionalized proteins in the irradiated regions of the network. Aromatic aldehydes were introduced to the model protein bovine serum albumin (BSA, MW = 66,463 Da, 60 primary amines) by treatment either with 2,5-dioxopyrrolidin-1-yl 4-formylbenzoate (NHS-CHO) or with 2,5-dioxopyrrolidin-1-yl 4-(4-(1-((4-(4-formylbenzamido)butanoyl)oxy)ethyl)-2-methoxy-5-nitrophenoxy)butanoate (NHS-*o*NB-CHO, Fig. 1c and Supplementary Methods 5–7). The *N*-hydroxysuccinimide (NHS) esters react with primary amines on lysine side chains and at the *N*-terminus to form stable amide linkages. The reaction proceeds under physiological conditions and represents the most common chemistry by which PEGylated therapeutics are generated from fragile proteins (for example, Pegademase, Pegvisomant, Pegaspargase)[45]. Model studies suggested a degree of functionalization of 3.8%, corresponding to an average of ~2.25 aldehydes per protein (Supplementary Fig. 4). Aldehyde-functionalized BSA was further tagged with an Alexa Fluor 488 fluorophore, yielding patternable protein denoted as BSA_{488}-*o*NB-CHO, such that gel-bound protein could be visualized and quantified with fluorescence microscopy (Supplementary Fig. 5).

In a typical patterning experiment, hydrogels containing photocaged alkoxyamines (100 μM) were exposed to light and sub-

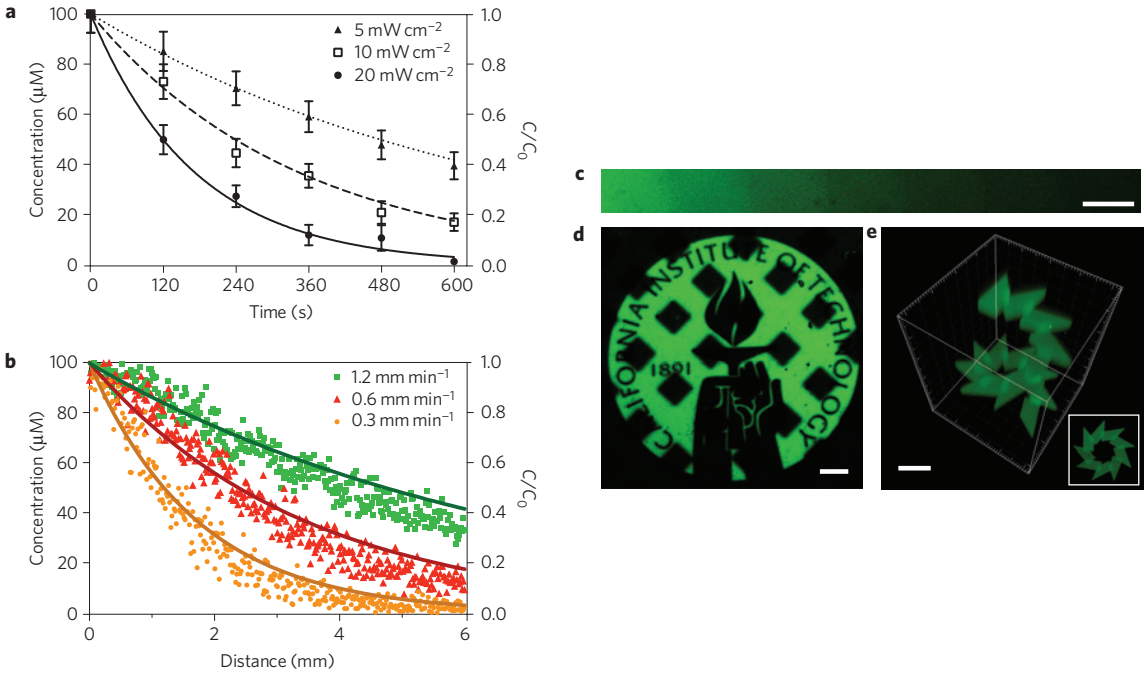

Figure 3 | Photoremoval of pre-patterned proteins from SPAAC-based gels through *o*-nitrobenzyl ester linker photocleavage. Immobilized proteins of interest are released from the hydrogel on *o*-nitrobenzyl ester (*o*NB) photocleavage. **a**, By regulating the degree of *o*NB photocleavage through variation in light intensity (5, 10, 20 mW cm^{-2}, $\lambda = 365$ nm) and exposure time (0–600 s), photorelease was controlled within wide limits. Data points in **a** correspond to mean values of three independent experimental replicates. Error bars correspond to the standard deviation about the mean. **b**,**c**, By subjecting uniformly functionalized hydrogels to linear gradients of light exposure (created by covering samples with an opaque photomask moving at rates of 0.3, 0.6, or 1.2 mm min^{-1}), exponential protein gradients were generated in a predictable manner. **d**,**e**, Subsets of immobilized proteins were removed by patterned exposure to UV light ($\lambda = 365$ nm or 740 nm). All studies were performed with pre-patterned BSA$_{488}$-*o*NB-CHO ($C_0 = 100$ μM); samples were imaged by fluorescence confocal microscopy. In **a**,**b**, lines represent predicted immobilization concentrations based on *o*NB photoscission kinetics. Inset in **e** represents a maximum-intensity *z*-projection. Scale bars, 500 μm (**c**), 100 μm (**d**) and 150 μm (**e**).

sequently incubated overnight in buffered solutions containing aldehyde-functionalized BSA. The gels were washed to remove unconjugated reactants, and examined by fluorescence confocal microscopy to visualize and quantify the degree of covalent protein attachment. Experimentally determined concentrations of immobilized BSA spanned the full range defined by the initial concentration of N_3–TEG–ONH–NPPOC in the gel, and were in excellent agreement with the levels of uncaging predicted from the light intensity (5, 10, 20 mW cm^{-2}) and exposure time (0–300 s) (Fig. 2a). Moreover, a simple dose dependence for the photomediated oxime ligation was observed, where the extent of hydrogel labelling varied only with the number of incident photons (Supplementary Fig. 6). The dose-dependent response was exploited to create gradients in the concentration of grafted proteins; linear gradients in the dose yielded controlled exponential gradients in concentration (Fig. 2b,c). Collimated light ($\lambda = 365$ nm, 10 mW cm^{-2}) was directed onto the substrate and partially shielded with an opaque photomask that was moved at various rates (0.6, 1.2, 2.4 mm min^{-1}) across the sample to create exposure gradients (Supplementary Fig. 7). More complex protein patterns were generated by traditional photolithographic techniques, where 2D geometric shapes defined by photomasks were patterned throughout the gel thickness (Fig. 2d). Furthermore, full-length proteins were immobilized in the gel with good 3D control (~1 μm resolution in the x–y plane, ~3–5 μm along the z-axis) by using a multiphoton laser-scanning lithographic approach (Fig. 2e and Supplementary Movie 1). By varying the pulsed laser conditions (that is, repeat numbers, laser power), excellent control over the extent of biochemical labelling was obtained for 3D patterning (Supplementary Fig. 8).

Treatment of BSA with NHS-*o*NB-CHO was used to outfit the protein with reactive aromatic aldehydes tethered by photolabile ortho-nitrobenzyl ester (*o*NB) linkers. The carbonyl functionality permits proteins to be conjugated to photodeprotected alkoxyamines within the hydrogel, and the *o*NB linker enables their subsequent photorelease (Supplementary Fig. 9). On mild UV exposure ($\lambda = 365$ nm), the *o*NB moiety undergoes irreversible cleavage (Figs 1e and 3), following first-order kinetics ($\phi = 0.02$, $\varepsilon = 4{,}780$ M^{-1} cm^{-1} for $\lambda = 365$ nm; ref. 17) and enabling release of the protein to be predicted accurately as a function of exposure. After immobilization at a fixed concentration (100 μM), BSA was released in controlled fashion on irradiation at various intensities (5, 10, 20 mW cm^{-2}) and exposure times (0–600 s) (Fig. 3a). The dose dependence of the photorelease step (Supplementary Fig. 10) was again exploited to prepare exponential gradients in the protein concentration (Fig. 3b,c). Protein patterns generated by photomediated oxime ligation (Fig. 2d,e) could be altered by protein removal either by means of irradiation through masks or through the use of focused laser pulses (Fig. 3d,e and Supplementary Movie 2). Moreover, the extent of protein removal was readily controlled in 3D by varying the multiphoton laser-scanning conditions (that is, number of repeats, laser power) for a given scan speed (Supplementary Fig. 11).

Because NPPOC uncaging and *o*NB photolysis can be initiated with the same light source, photorelease of a first patterned protein can be performed in concert with the photomediated ligation of a second protein to create complex, interconnected biochemical patterns (Fig. 4a). For example, uniform introduction of a photoreleasable protein throughout the gel at a concentration half that of the N_3–TEG–ONH–NPPOC linker, followed by photorelease and subsequent immobilization of a second protein, yields intricate interconnected patterns in which the two proteins are present at equal concentrations. As shown in Fig. 4b,c, we prepared patterns

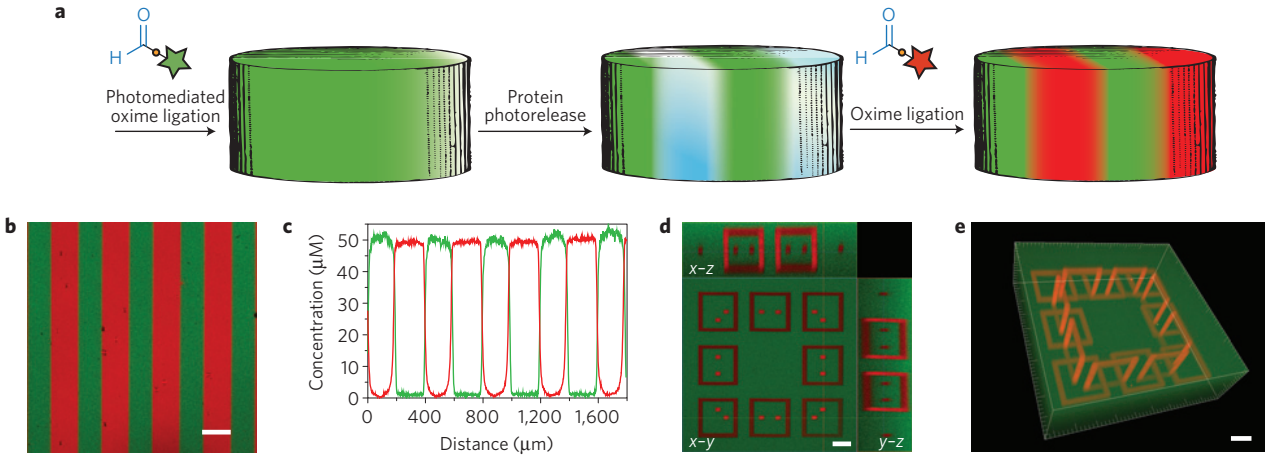

Figure 4 | Interconnected dual-protein patterns generated through protein photorelease and oxime ligation. a, Because the chemistries used for protein tethering and excision (that is, NPPOC uncaging and *o*NB photolysis) can be initiated with the same light sources, interconnected biochemical patterns can be generated by carrying out these processes simultaneously. If protein attachment by means of photomediated oxime ligation is performed without complete alkoxyamine deprotection, the surviving NPPOC moieties will be uncaged concurrently with release of the first protein on a second round of light exposure. This procedure results in the creation of anchoring sites for further protein immobilization in the regions of photorelease. If the first protein is fully removed from the volumes exposed in the second round, patterned proteins are immobilized within mutually exclusive subvolumes of the gel. **b**,**c**, Masked light ($\lambda = 365$ nm) was used to generate interspaced line patterns of two fluorescently labelled proteins at equal concentrations extending throughout the gel with minimal overlap. **d**,**e**, Dual-protein patterning was performed using pulsed laser light ($\lambda = 740$ nm) to create interlocked chains of a red protein in a sea of green. All studies were performed with pre-patterned protein BSA_{488}-*o*NB-CHO (green, 50 μM) and secondary protein BSA_{594}-*o*NB-CHO (red). Gels were imaged by fluorescence confocal microscopy. Scale bars, 200 μm (**b**) and 50 μm (**d**,**e**).

of alternating lines (width = 200 μm) of two fluorescently labelled proteins (BSA_{488}-*o*NB-CHO and BSA_{594}-*o*NB-CHO), in which the total protein concentration remained constant across the material and overlap of functionalized regions was minimal (Supplementary Fig. 12). In a second example, multiphoton laser scanning was used to create interlocking chains of one protein enclosed within another (Fig. 4d,e and Supplementary Fig. 13 and Supplementary Movie 3).

The methods described here will be most useful if the times required for patterning are comparable to or shorter than those characteristic of the cellular processes that the investigator wants to control. With respect to the kinetics of protein immobilization, both protein diffusion and formation of the oxime linkage must be considered. Oxime formation between aromatic aldehydes and alkoxyamines is relatively fast, exhibiting a second-order rate constant of the order of $10\,M^{-1}\,s^{-1}$ (refs 46,47). We used fluorescence recovery after photobleaching (FRAP) to determine the diffusion coefficient for BSA within the PEG hydrogel. Consistent with previous findings in PEG networks formed through Michael-type addition chemistry[48], we found a diffusion coefficient of $\sim 1.8 \times 10^{-11}\,m^2\,s^{-1}$, roughly a quarter of that of BSA in water[49] (Supplementary Fig. 14). We incorporated these kinetic parameters into a reaction–diffusion model, and solved it numerically to examine the time required for biomacromolecular patterning (Supplementary Fig. 15). For gels of moderate thickness (1 mm) covalently attached to glass, the process is diffusion limited, and the top 80% of the gel is predicted to be >90% functionalized after 6.5 h, indicating that the overnight protein patterning steps used in this work were sufficient to achieve near-complete reaction throughout the gel. For thin gels (<200 μm), protein immobilization is reaction limited, and the minimum time required for protein immobilization is approximately 2 h. Patterning gels over volumes significantly larger than that of a typical mammalian cell (~10 μm diameter) can thus be accomplished within a few hours—fast enough to be useful in regulating a variety of important biological functions, including proliferation, migration and differentiation.

We next sought to determine whether protein biofunctionality was preserved throughout the photoreversible gel patterning process. Specifically, we evaluated the activity of three further patterned proteins, each of a different functional class: the enzyme collagenase, a mouse anti-6xHis monoclonal antibody, and growth factor Delta (Fig. 5 and Supplementary Methods 7). For enzyme studies, collagenase-modified gels were treated with a self-quenched fluorogenic peptide probe[15] (FAM-RGL↓GPAGRK(FAM)-NH_2) whose fluorescence increases by an approximate factor of eight on its enzymatic cleavage (Fig. 5a,b and Supplementary Methods 8 and Supplementary Fig. 16). Collagenase-functionalized gels yielded increased solution fluorescence, corresponding to conserved enzymatic activity. On subsequent light exposure, photoreleased collagenase remained active in solution. We estimate that collagenase retained ~58% of its original bioactivity on NHS-*o*NB-CHO labelling, ~24% on gel immobilization, and ~47% on photomediated release (Supplementary Fig. 17). For antibody recognition studies, mouse anti-6xHis primary antibody was patterned into gels by photomediated oxime ligation (Fig. 5c,d). Some of these patterned gels were then exposed to a second dosage of masked light to photorelease portions of the patterned primary antibody. The remaining gel-bound primary antibody was visualized with a fluorescent secondary antibody (Alexa Fluor 488-conjugated goat anti-mouse antibody). The photolithographically defined pattern in fluorescence indicates that the gel-bound primary antibody remained recognizable to the secondary antibody. Finally, to demonstrate the bioactivity of growth factors immobilized into the gel, we examined the upregulation of the Notch signalling pathway by Delta[50] (Fig. 5e,f). Notch luciferase reporter human osteosarcoma U2OS cells[51] were cultured on Delta-functionalized gels for 48 h. Notch-driven luciferase activity was found to be approximately twice as high for cells cultured on Delta-functionalized materials as for those lacking the growth factor. Consistent with previous findings that substrate–Delta tethering is required for Notch activation[52], no increase in Notch signalling was observed when cells were cultured in the presence of soluble Delta. Taken together, these studies indicate that protein bioactivity can be maintained throughout NHS-*o*NB-CHO labelling and gel patterning processes.

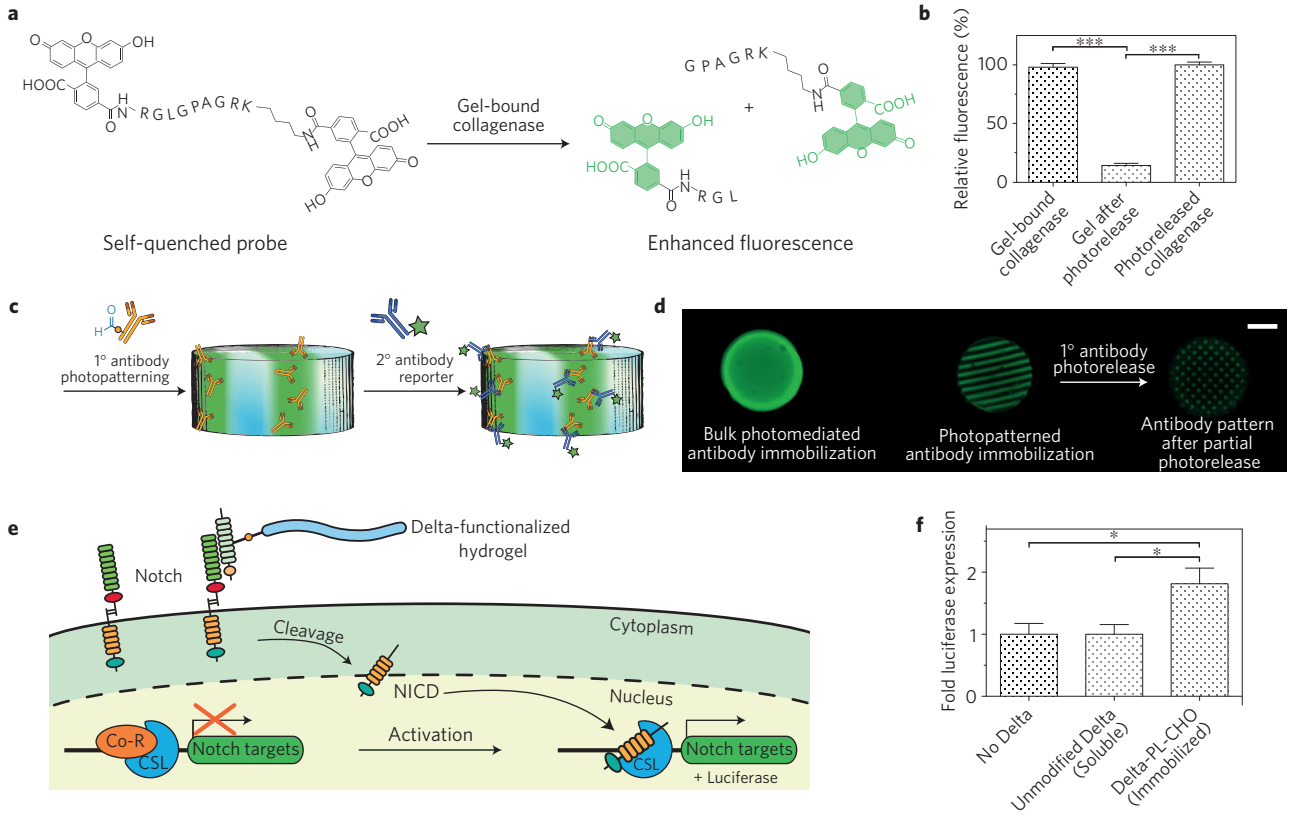

Figure 5 | Proteins remain bioactive on photoreversible patterning of gels. a, The self-quenched FAM-RGL↓GPAGRK(FAM)-NH_2 peptide probe, whose fluorescence increases significantly on enzymatic cleavage, serves as a fluorogenic reporter of collagenase activity. **b**, Such enzymatic activity remains high for both gel-immobilized and photoreleased collagenase. Data is plotted as mean; error bars are standard error of mean; *** denotes $p < 0.001$. **c**,**d**, Patterned primary antibodies are visualized with a fluorescent secondary antibody, indicating that the gel-bound primary antibody remained functionally recognizable to the secondary antibody. **e**, Tethered Delta interacts with surface Notch receptor to trigger two proteolytic cleavages that release Notch intracellular domain (NICD) from the plasma membrane. NICD undergoes nuclear translocation and converts the CSL transcriptional repressor to an activator. This activation promotes Notch-mediated signalling and, in the case of the used U2OS Notch reporter cell line, luciferase expression. **f**, U2OS reporter cells cultured on Delta-functionalized gels exhibit enhanced Notch signalling compared with unfunctionalized gels, with or without the addition of soluble Delta. Data is plotted as mean; error bars are standard error of mean; * denotes $p < 0.05$. Scale bar, 3 mm (**d**).

To evaluate the utility of reversible, photomediated presentation of protein ligands in controlling cellular behaviour, we focused on directing osteogenic differentiation of human mesenchymal stem cells (hMSCs). It has recently been shown that hMSCs undergo osteogenesis when cultured in 3D environments that permit cell spreading[53]. Here we examined the response of hMSCs to spreading cues that vary in time. Specifically, we controlled the adhesive character of the PEG network through photoreversible patterning of vitronectin (VTN, MW = 75 kDa), an abundant glycoprotein that promotes cell spreading[54]. In 2D control experiments, we confirmed that hMSCs seeded on the surfaces of PEG gels exhibit no attachment in the absence of VTN. In contrast, cells seeded on VTN-patterned materials bound preferentially to the functionalized areas of the surface (Supplementary Fig. 18), and could be detached on VTN photorelease. In complementary 3D culture studies (Fig. 6), hMSC-laden gels were labelled with VTN-*o*NB-CHO (100 μM) after one day of culture to induce spreading. On day 4, gels were exposed to UV light to release VTN. Osteogenic differentiation was assessed on days 1, 4 and 10, by osteocalcin (OC) immunostaining and by assaying for alkaline phosphatase (ALP) activity. Consistent with the results in ref. 53, hMSCs cultured in environments that do not support cell spreading (that is, without VTN) did not undergo osteogenesis. In contrast, after introduction of VTN on day 1, samples analysed on day 4 exhibited significantly increased ALP activity and OC production. Interestingly, after the VTN cue was removed (on day 4), OC production and ALP activity returned to their pre-differentiated levels by day 10. Although our initial studies were performed in uniform gels (Fig. 6b–e), similar results were observed in patterned materials (Fig. 6f–i). Specifically, osteogenesis was confined to gel volumes that contained VTN (which was patterned in the form of 150-μm-wide 'lines' extending throughout the 1-mm-thick gels). On patterned removal of the adhesive protein, square islands (150 μm × 150 μm × 1 mm) of VTN were left intact, and OC production at day 10 was maintained in VTN-functionalized gel subvolumes but not in the photoreleased portions of the material (Supplementary Movie 4). High cell viability was maintained throughout both patterning reactions (Supplementary Fig. 19). Although future studies are required to discern the effects of cell/physical material attachment and VTN-mediated protein signalling on hMSC fate, we believe that these results represent the first demonstration of user-directed, spatially controlled, reversible stem cell differentiation in 3D.

The results described here illustrate a general strategy for gaining spatial and temporal control of protein presentation in 3D cell culture. Through a combination of bioorthogonal, light-based chemistries, bioactive proteins can be introduced to, and removed from, engineered hydrogels on timescales of a few hours and with spatial resolution well below the characteristic dimensions of mammalian cells. Moreover, such reversible biochemical alteration is performed in a manner that is fully independent of network

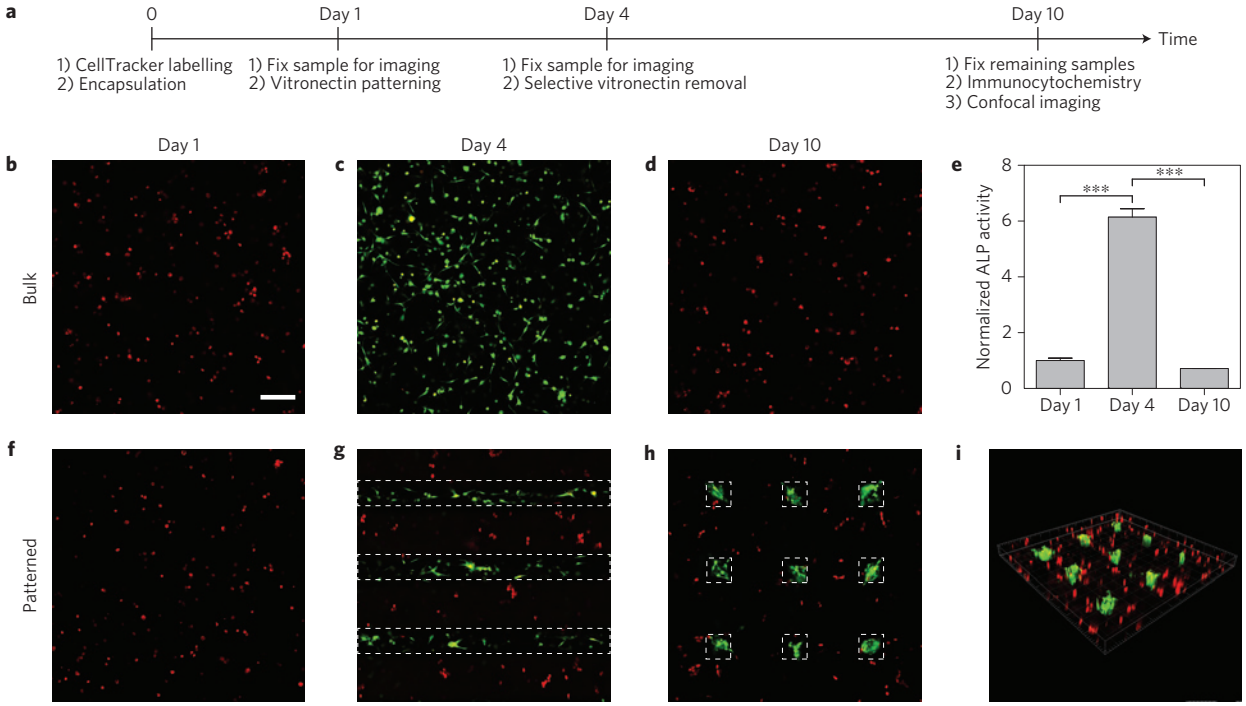

Figure 6 | Spatial and temporal control of hMSC differentiation by photoreversible patterning of vitronectin. a, hMSCs were labelled with CellTracker Red and encapsulated (3×10^6 cells ml^{-1}) in enzymatically degradable SPAAC-based networks. On day 1, vitronectin (VTN, 100 μM) was patterned into hydrogels by means of photomediated oxime ligation to induce cell spreading. Culture was continued for three more days, after which VTN was photoreleased. Cells were maintained in culture until day 10. hMSC differentiation was assessed by immunocytochemical staining for osteocalcin (OC, green) and by alkaline phosphatase (ALP) activity assays, on days 1, 4 and 10. **b**–**e**, For uniformly functionalized gels, cells exhibited limited interaction with the hydrogel matrix before the introduction of VTN on day 1, after which cells stained positive for OC and exhibited increased ALP activity. After VTN photorelease on day 4, cells returned to a spherical unbound state and exhibited marked decreases in OC staining and ALP activity. **f**–**i**, For hydrogels containing spatially patterned VTN, OC-positive staining was confined to VTN-functionalized portions of the material (indicated by dashed rectangles). On patterned removal of the adhesive protein, staining for OC was observed only in VTN islands. Images in **b**–**d** and **f**–**h** represent single *z*-slices from fluorescence confocal microscopy. ALP activity assays in **e** are normalized to the value on day 1. In **e** data is plotted as mean; error bars are standard error of mean; *** denotes $p < 0.001$. Scale bar, 200 μm.

mechanics, enabling the effects of dynamic biochemical cues to be assayed independently from material stiffness. We expect that this approach will prove useful in expanding our understanding of how cells respond to extracellular cues, and in the design of materials for use in tissue engineering and regenerative medicine.

Methods

Formation of SPAAC-based hydrogels. A solution of PEG-tetraBCN (7.3 mM), N_3–DGPQGIWGQGDK(N_3)–NH_2 (14.6 mM) and N_3–TEG–ONH–NPPOC (100 μM) was prepared in phosphate-buffered saline (PBS, pH = 7.4). The gel precursor solution was allowed to react for 30 min (Supplementary Fig. 1) between azide-functionalized (Supplementary Methods 3) and Rain-X-treated glass slides spaced with 1-mm-thick silicone rubber (McMaster-Carr). The slides were separated, and the resulting gels were swollen overnight in PBS before use.

Photopatterning conditions for immobilization or release of proteins. For photolithographic patterning, hydrogels were exposed through a patterned chrome photomask (Photo Sciences) to collimated UV light ($\lambda = 365$ nm, 5–20 mW cm^{-2}, 0–600 s) emanating from a Lumen Dynamics OmniCure S1500 Spot UV Curing system equipped with an internal 365 nm band-pass filter. Alternatively, multiphoton absorption laser-scanning lithography was used to initiate 3D photomediated protein ligation or photorelease. Here, regions of interest (x–y ROI) were scanned at 1 μm z-axis increments with pulsed laser light ($\lambda = 740$ nm, power = 25–100% with max power = 1,350 mW μm^{-2}, scan speed = 2.07 μs μm^{-2}, scan repeats = 1–16) on a Zeiss LSM 510 Meta NLO equipped with a 20× Fluar objective (NA = 0.75, Zeiss) and a Coherent Chameleon multiphoton laser. By scanning different sets of ROIs at user-defined z-positions within the material, 3D patterns were obtained (this process is discussed in greater detail elsewhere[30]). After NPPOC photolysis from the initial light exposure, gels were gently agitated overnight on an orbital shaker in PBS containing 200 μM aldehyde-functionalized protein (for example, BSA_{488}*o*NB-CHO, VTN-CHO) and 4-amino-L-phenylalanine[47] (10 mM). The gels were washed with PBS (12 h) before visualization by fluorescence confocal microscopy. In the case of *o*NB-CHO-functionalized proteins, a second light exposure was employed to induce photoremoval, after which gels were washed with PBS for 12 h before fluorescence imaging. Phenol-red-free medium was substituted for PBS when patterning experiments were performed in the presence of live cells.

Notch activity assays. Human osteosarcoma U2OS Notch CSL Luciferase/Renilla reporter cells (generously provided by K. Beres, C. Murry, J. Berndt and the Moon laboratory at the University of Washington) were cultured in DMEM supplemented with 10% foetal bovine serum, 2 mM L-glutamine, 100 U ml^{-1} penicillin and 100 μg ml^{-1} streptomycin. Cells were seeded on Delta-functionalized gels and cultured with or without soluble Delta (100 μg ml^{-1}) for 48 h in 5% CO_2 at 37 °C. The gels were rinsed, trypsinized and lysed in 1× passive lysis buffer (Promega). A Dual-Luciferase reporter assay kit (Promega) was further used to quantify Notch activation following manufacturer protocols.

hMSC culture conditions. Adult human mesenchymal stem cells (hMSCs) isolated from bone marrow aspirate were obtained from Lonza. hMSCs were expanded in a growth medium formulation consisting of low-glucose DMEM (Invitrogen) containing 10% foetal bovine serum and 1% penicillin/streptomycin. Cells were labelled with CellTracker Orange CMRA (5 μM in serum-free low-glucose DMEM, Invitrogen) according to the manufacturer's protocol. hMSCs (passage 3) were encapsulated in SPAAC-based gels (10 wt%) at 3×10^6 cells ml^{-1} and cultured in StemXVivo Human Osteogenic Inductive medium (R&D Systems) supplemented with 1% penicillin/streptomycin. The medium was changed every two to three days. Cells were incubated in 5% CO_2 at 37 °C.

Evaluation of hMSC differentiation fate. Immunocytochemical evaluation of hMSC differentiation. Cell-laden gels were fixed in aqueous paraformaldehyde (3.7% in PBS, pH = 7.4) for 1 h at 25 °C. Samples were washed (3% BSA in PBS),

permeabilized (0.5% Triton X-100 in PBS for 2 h), and blocked with BSA (3% in PBS) for 1 h. Constructs were incubated overnight at 4 °C with a mouse anti-OC primary antibody (1:10 dilution, IgG, R&D Systems), washed with PBS, and incubated with an Alexa Fluor 488-conjugated goat anti-mouse antibody (1:200 dilution, Invitrogen) before visualization by fluorescence confocal microscopy. Alkaline phosphatase (ALP) activity assay. ALP activity was assayed following a published procedure[55]. Briefly, hMSC-laden gels were first incubated in medium containing alamarBlue Reagent (10%, Invitrogen) for 4 h. Supernatant fluorescence was determined (560 nm excitation, 590 nm emission) and used as a measure of the number of viable cells within the samples. Gels were then rinsed with PBS and homogenized manually in CelLytic M cell lysis buffer. Supernatants were treated with *p*-nitrophenyl phosphate (1:1 sample:*p*−NPP solution) for 10 min and quenched with aqueous sodium hydroxide (3 M). Normalized ALP activity was reported as the sample absorbance ($\lambda = 405$ nm) divided by the alamarBlue fluorescence signal.

Received 15 July 2014; accepted 15 January 2015; published online 23 February 2015

References

1. DeForest, C. A. & Anseth, K. S. Advances in bioactive hydrogels to probe and direct cell fate. *Annu. Rev. Chem. Biomol.* **3,** 421–444 (2012).
2. Langer, R. & Tirrell, D. A. Designing materials for biology and medicine. *Nature* **428,** 487–492 (2004).
3. Lutolf, M. P., Gilbert, P. M. & Blau, H. M. Designing materials to direct stem-cell fate. *Nature* **462,** 433–441 (2009).
4. Engler, A. J., Sen, S., Sweeney, H. L. & Discher, D. E. Matrix elasticity directs stem cell lineage specification. *Cell* **126,** 677–689 (2006).
5. Huebsch, N. *et al.* Harnessing traction-mediated manipulation of the cell/matrix interface to control stem-cell fate. *Nature Mater.* **9,** 518–526 (2010).
6. Yang, C., Tibbitt, M. W., Basta, L. & Anseth, K. S. Mechanical memory and dosing influence stem cell fate. *Nature Mater.* **13,** 645–652 (2014).
7. Chen, C. S., Mrksich, M., Huang, S., Whitesides, G. M. & Ingber, D. E. Geometric control of cell life and death. *Science* **276,** 1425–1428 (1997).
8. Petersen, O. W., Ronnovjessen, L., Howlett, A. R. & Bissell, M. J. Interaction with basement-membrane serves to rapidly distinguish growth and differentiation pattern of normal and malignant human breast epithelial cells. *Proc. Natl Acad. Sci. USA* **89,** 9064–9068 (1992).
9. Burdick, J. A. & Murphy, W. L. Moving from static to dynamic complexity in hydrogel design. *Nature Commun.* **3,** 1269 (2012).
10. Lutolf, M. P. & Hubbell, J. A. Synthetic biomaterials as instructive extracellular microenvironments for morphogenesis in tissue engineering. *Nature Biotechnol.* **23,** 47–55 (2005).
11. Rompolas, P., Mesa, K. R. & Greco, V. Spatial organization within a niche as a determinant of stem-cell fate. *Nature* **502,** 513–518 (2013).
12. Katz, J. S. & Burdick, J. A. Light-responsive biomaterials: Development and applications. *Macromol. Biosci.* **10,** 339–348 (2010).
13. DeLong, S. A., Moon, J. J. & West, J. L. Covalently immobilized gradients of bFGF on hydrogel scaffolds for directed cell migration. *Biomaterials* **26,** 3227–3234 (2005).
14. Hahn, M. S., Miller, J. S. & West, J. L. Three-dimensional biochemical and biomechanical patterning of hydrogels for guiding cell behavior. *Adv. Mater.* **18,** 2679–2684 (2006).
15. DeForest, C. A., Polizzotti, B. D. & Anseth, K. S. Sequential click reactions for synthesizing and patterning three-dimensional cell microenvironments. *Nature Mater.* **8,** 659–664 (2009).
16. DeForest, C. A., Sims, E. A. & Anseth, K. S. Peptide-functionalized click hydrogels with independently tunable mechanics and chemical functionality for 3D cell culture. *Chem. Mater.* **22,** 4783–4790 (2010).
17. DeForest, C. A. & Anseth, K. S. Cytocompatible click-based hydrogels with dynamically tunable properties through orthogonal photocoupling and photodegradation reactions. *Nature Chem.* **3,** 925–931 (2011).
18. Luo, Y. & Shoichet, M. S. A photolabile hydrogel for guided three-dimensional cell growth and migration. *Nature Mater.* **3,** 249–253 (2004).
19. Wylie, R. G. *et al.* Spatially controlled simultaneous patterning of multiple growth factors in three-dimensional hydrogels. *Nature Mater.* **10,** 799–806 (2011).
20. Adzima, B. J. *et al.* Spatial and temporal control of the alkyne–azide cycloaddition by photoinitiated Cu(II) reduction. *Nature Chem.* **3,** 258–261 (2011).
21. Mosiewicz, K. A. *et al. In situ* cell manipulation through enzymatic hydrogel photopatterning. *Nature Mater.* **12,** 1072–1078 (2013).
22. Kloxin, A. M., Kasko, A. M., Salinas, C. N. & Anseth, K. S. Photodegradable hydrogels for dynamic tuning of physical and chemical properties. *Science* **324,** 59–63 (2009).
23. Wirkner, M. *et al.* Triggered cell release from materials using bioadhesive photocleavable linkers. *Adv. Mater.* **23,** 3907–3910 (2011).
24. Griffin, D. R. *et al.* Synthesis of photodegradable macromers for conjugation and release of bioactive molecules. *Biomacromolecules* **14,** 1199–1207 (2013).
25. Kloxin, A. M., Tibbitt, M. W. & Anseth, K. S. Synthesis of photodegradable hydrogels as dynamically tunable cell culture platforms. *Nature Protoc.* **5,** 1867–1887 (2010).
26. Fairbanks, B. D., Singh, S. P., Bowman, C. N. & Anseth, K. S. Photodegradable, photoadaptable hydrogels via radical-mediated disulfide fragmentation reaction. *Macromolecules* **44,** 2444–2450 (2011).
27. Griffin, D. R. & Kasko, A. M. Photodegradable macromers and hydrogels for live cell encapsulation and release. *J. Am. Chem. Soc.* **134,** 13103–13107 (2012).
28. Azagarsamy, M. A., Alge, D. L., Radhakrishnan, S. J., Tibbitt, M. W. & Anseth, K. S. Photocontrolled nanoparticles for on-demand release of proteins. *Biomacromolecules* **13,** 2219–2224 (2012).
29. He, M., Li, J., Tan, S., Wang, R. & Zhang, Y. Photodegradable supramolecular hydrogels with fluorescence turn-on reporter for photomodulation of cellular microenvironments. *J. Am. Chem. Soc.* **135,** 18718–18721 (2013).
30. DeForest, C. A. & Anseth, K. S. Photoreversible patterning of biomolecules within click-based hydrogels. *Angew. Chem. Int. Ed.* **51,** 1816–1819 (2011).
31. Lutolf, M. P. Materials science: Cell environments programmed with light. *Nature* **482,** 477–478 (2012).
32. Alge, D. L. & Anseth, K. S. Bioactive hydrogels: Lighting the way. *Nature Mater.* **12,** 950–952 (2013).
33. Agard, N. J., Prescher, J. A. & Bertozzi, C. R. A strain-promoted [3+2] azide-alkyne cycloaddition for covalent modification of biomolecules in living systems. *J. Am. Chem. Soc.* **126,** 15046–15047 (2004).
34. Lutolf, M. P. *et al.* Synthetic matrix metalloproteinase-sensitive hydrogels for the conduction of tissue regeneration: Engineering cell-invasion characteristics. *Proc. Natl Acad. Sci. USA* **100,** 5413–5418 (2003).
35. Patterson, J. & Hubbell, J. A. Enhanced proteolytic degradation of molecularly engineered PEG hydrogels in response to MMP-1 and MMP-2. *Biomaterials* **31,** 7836–7845 (2010).
36. Codelli, J. A., Baskin, J. M., Agard, N. J. & Berozzi, C. R. Second-generation difluorinated cyclooctynes for copper-free click chemistry. *J. Am. Chem. Soc.* **130,** 11486–11493 (2008).
37. Sims, E. A., DeForest, C. A. & Anseth, K. S. A mild, large-scale synthesis of 1,3-cyclooctanedione: Expanding access to difluorinated cyclooctyne for copper-free click chemistry. *Tetrahedron Lett.* **52,** 1871–1873 (2011).
38. Ning, X. H., Guo, J., Wolfert, M. A. & Boons, G. J. Visualizing metabolically labeled glycoconjugates of living cells by copper-free and fast huisgen cycloadditions. *Angew. Chem. Int. Ed.* **47,** 2253–2255 (2008).
39. Debets, M. F. *et al.* Aza-dibenzocyclooctynes for fast and efficient enzyme PEGylation via copper-free (3+2) cycloaddition. *Chem. Commun.* **46,** 97–99 (2010).
40. Tibbitt, M. W., Kloxin, A. M., Sawicki, L. A. & Anseth, K. S. Mechanical properties and degradation of chain and step-polymerized photodegradable hydrogels. *Macromolecules* **46,** 2785–2792 (2013).
41. Dendane, N. *et al.* Efficient surface patterning of oligonucleotides inside a glass capillary through oxime bond formation. *Bioconjug. Chem.* **18,** 671–676 (2007).
42. Park, S. & Yousaf, M. N. An interfacial oxime reaction to immobilize ligands and cells in patterns and gradients to photoactive surfaces. *Langmuir* **24,** 6201–6207 (2008).
43. Woll, D. *et al.* Intramolecular sensitization of photocleavage of the photolabile 2-(2-nitrophenyl)propoxycarbonyl (NPPOC) protecting group: Photoproducts and photokinetics of the release of nucleosides. *Chem. Eur. J.* **14,** 6490–6497 (2008).
44. Odian, G. G. *Principles of Polymerization* 4th edn (Wiley-Interscience, 2004).
45. Jevševar, S., Kunstelj, M. & Porekar, V. G. PEGylation of therapeutic proteins. *Biotechnol. J.* **5,** 113–128 (2010).
46. Dirksen, A. & Dawson, P. E. Rapid oxime and hydrazone ligations with aromatic aldehydes for biomolecular labeling. *Bioconjug. Chem.* **19,** 2543–2548 (2008).
47. Blanden, A. R., Mukherjee, K., Dilek, O., Loew, M. & Bane, S. L. 4-aminophenylalanine as a biocompatible nucleophilic catalyst for hydrazone ligations at low temperature and neutral pH. *Bioconjug. Chem.* **22,** 1954–1961 (2011).
48. Zustiak, S. P. & Leach, J. B. Characterization of protein release from hydrolytically degradable poly(ethylene glycol) hydrogels. *Biotechnol. Bioeng.* **108,** 197–206 (2011).
49. Phillies, G. D. Diffusion of bovine serum albumin in a neutral polymer solution. *Biopolymers* **24,** 379–386 (1985).
50. Kopan, R. & Ilagan, M. X. G. The canonical Notch signaling pathway: Unfolding the activation mechanism. *Cell* **137,** 216–233 (2009).

51. Beckstead, B. L., Santosa, D. M. & Giachelli, C. M. Mimicking cell–cell interactions at the biomaterial-cell interface for control of stem cell differentiation. *J. Biomed. Mater. Res. A* **79A,** 94–103 (2006).
52. Varnum-Finney, B. *et al.* Immobilization of Notch ligand, Delta-1, is required for induction of Notch signaling. *J. Cell Sci.* **113,** 4313–4318 (2000).
53. Khetan, S. *et al.* Degradation-mediated cellular traction directs stem cell fate in covalently crosslinked three-dimensional hydrogels. *Nature Mater.* **12,** 458–465 (2013).
54. Hayman, E. G., Pierschbacher, M. D., Ohgren, Y. & Ruoslahti, E. Serum spreading factor (vitronectin) is present at the cell surface and in tissues. *Proc. Natl Acad. Sci. USA* **80,** 4003–4007 (1983).
55. Lin, C. C., Metters, A. T. & Anseth, K. S. Functional PEG-peptide hydrogels to modulate local inflammation induced by the pro-inflammatory cytokine TNFα. *Biomaterials* **30,** 4907–4914 (2009).

Acknowledgements

The authors thank P. Rapp for discussions on FRAP and FEM analysis, as well as for his constructive comments on the manuscript; M. Shahgholi and N. Torian for assistance with HRMS; J. Heath, J. Pfeilsticker and R. Henning for advice on peptide work and for use of their peptide synthesizer and HPLC; D. Koos and the Caltech Biological Imaging Center for use of confocal microscopes; and K. Beres and C. Murry for assistance with all Notch-related studies. This work was supported by the National Science Foundation Grant NSF-DMR 1206121 and a University of Washington Faculty Startup Grant (C.A.D.).

Author contributions

C.A.D. and D.A.T. designed the experiments. C.A.D. conducted the experiments. C.A.D. and D.A.T. interpreted the data and composed the manuscript.

Additional information

Supplementary information is available in the online version of the paper. Reprints and permissions information is available online at www.nature.com/reprints. Correspondence and requests for materials should be addressed to C.A.D. or D.A.T.

Competing financial interests

The authors declare no competing financial interests.